Electronic Supplementary Material (ESI) for Journal of Materials Chemistry C.

Supporting Information **for**

A multi-responsive luminescent Co(II) coordination polymer assembled from amide-functionalized organic units for effective pH and cation sensing

Luyao Wang#[a], Xiao Sun#[a], Jiawei Cheng[a], Jing Lu[a], Yunwu Li[a], Jianmin Dou[a], Haiquan Tian[a]*, Suna Wang[a]*

[a] Shandong Provincial Key Laboratory of Chemical Energy Storage and Novel Cell Technology, School of Chemistry and Chemical Engineering, Liaocheng University, Liaocheng 252059, People's Republic of China.

Email: wangsuna@lcu.edu.cn; tianhaiquan@lcu.edu.cn

These authors contribute equally.

Table of Contents

Fig. S17 The detection limit of **LCU-112** toward Tb^{3+}.

Fig. S18 The luminescence emission of **LCU-112** in aqueous solutions containing different cations with the absence and presence of Tb^{3+} and Photo by 254 nm UV lamp.

Fig. S19 The recycling experimental of Tb^{3+} within five runs.

Fig. S20 Luminescence spectra of H_4L ligand and tttmb in aqueous solutions with Tb^{3+}.

Fig. S21 The titration experiment of Tb^{3+} solution into H_4L.

Fig. S22 (a) and (b) Fluorescence diagram and histogram of Tb^{3+} fluorescence sensing by H_4L under different pH conditions. (c) and (d) Fluorescence diagram and histogram of Tb^{3+} fluorescence sensing by **LCU-112** under different pH conditions.

Fig. S23 (a) and (b) The detection limit of **LCU-112** and **Tb^{3+}@LCU-112** toward Fe^{3+}.

Fig. S24 The time-dependent response of **LCU-112** and **Tb^{3+}@LCU-112** after adding Fe^{3+}.

Fig. S25 PXRD of **LCU-112** and **Tb^{3+}@LCU-112** soaked in aqueous solutions containing Fe^{3+} for three days.

Fig. S26 The excitation of **LCU-112** and **Tb^{3+}@LCU-112** and UV–Vis spectra of cations.

Fig. S27 (a) XPS spectra of **LCU-112** before and after immersion in Fe^{3+}. (b)-(f) High resolution regions of Co2p, Fe2p, C1s, O1s and N1s.

Fig. S28 (a) XPS spectra of **Tb^{3+}@LCU-112** before and after immersion in Fe^{3+}. (b)-(g) High resolution regions of Co2p, Tb3d, Fe2p, C1s, O1s and N1s.

Fig. S29 (a) The luminescence decay lifetimes of the original **LCU-112** and after soaked in aqueous solutions of Fe^{3+}. (b) The luminescence decay lifetimes of **Tb^{3+}@LCU-112** and after soaked in aqueous solutions of Fe^{3+}.

Materials and characterization.

The ligand H_4L was synthesized according to the reference [reference: H. Mehenni, H. Guillou, C. Tessier, J. Brisson, *Canadian Journal of Chemistry*, 2008, 86, 7-19.]. Other reagents were purchased and used without purity. The FT-IR spectra (4000–400 cm^{-1} region) were recorded from KBr pellets with a NICOLET 6700F-IR spectrometer. Elemental analyses of C, H and N were carried out with a vario EL cube elemental analyzer. Powder X-ray diffraction (PXRD) data were collected over the 2θ range of 5–50° using a SmartLab diffractometer with Cu Kα radiation (λ=1.5418 Å) at room temperature. Thermal analyses were performed on STA 449 F5 Jupiter instrument from room temperature to 800°C with a heating rate of 10°C/min under flowing nitrogen. Emission and excitation spectra in solid state as well as time-resolved luminescence were carried out on a FLS1000 spectrophotometer analyzer of Edinburgh instruments. Luminescence sensing properties were recorded on the Hitachi F-7000 Luminescence spectrophotometer. X-ray photoelectron spectroscopy (XPS) characterization was carried out by using a Thermo Fisher Scientific ESCALAB Xi+ spectrometer with Al Kα X-rays (1486.6 eV) as the light source. UV-vis measurements were conducted with a UH 4150 spectrophotometer. The EDS mapping were recorded with FIB Helios G4.

Synthesis of the Tb^{3+}@LCU-112.

20 mg samples of **LCU-112** were immersed in Tb^{3+} aqueous solutions (10^{-3} M, 10 mL) for three days. The post-synthesized sample of **Tb^{3+}@LCU-112** was obtained after filtration.

X-ray crystallographic study.

Single-crystal X-ray data for **LCU-112** were collected with an Agilent Xcalibur Eos Gemini CCD diffractometer at 293 K with Cu Kα radiation (λ = 1.54184 Å). The raw data frames were integrated into SHELX-format reflection files and corrected using SAINT program. Absorption corrections based on multi-scan were obtained by the SADABS program. The structure was solved with direct methods (SHELXS) and refined with full-matrix least-squares technique using the SHELXL-2018/3 programs. Displacement parameters were refined anisotropically, and the positions of the H-atoms were generated geometrically, assigned isotropic thermal parameters, and allowed to ride on their parent carbon atoms before the final cycle of refinement. Basic information pertaining to crystal parameters and structure refinement is summarized in Table S1. Selected bond lengths and angles are listed in Table S2.

Table S1. Crystal and refinement data for **LCU-112**.

LCU-112			
Empirical formula	$C_{30}H_{29}CoN_{10}O_6$	Formula weight	684.56
Temperature/ *K*	293	Crystal system	triclinic
Space group	$P\bar{1}$	Volume/Å^3	1468.4(4)
a [Å]	10.7536(17)	α [˚]	80.583(14)
b [Å]	11.7485(20)	β [˚]	79.812(13)
c [Å]	12.140(2)	γ [˚]	79.016(14)
Z	2	$D_{(calc.)}$ [g/cm^3]	1.548
μ [mm^{-1}]	5.131	θ range	3.733-67.232
Index ranges	$-12 \le h \le 12$ $-14 \le k \le 13$ $-10 \le l \le 14$	$^aR1;^bwR_2$ [$I > 2\sigma(I)$]	0.0520, 0.1287
		GOF	1.036

$^aR_1 = \Sigma| |F_o|-|F_c| | / \Sigma|F_o|$, $^bwR_2 = [\Sigma w(F_o^2-F_c^2)^2] / \Sigma w(F_o^2)^2]^{1/2}$

Table S2. Selected bond lengths [Å] and angles [º] for **LCU-112**.

LCU-112			
Co(1)-N(2)	2.122(3)	Co(1)-N(2)^1	2.122(3)
Co(1)-N(5)^2	2.191(3)	Co(1)-N(5)^3	2.191(3)
Co(1)-O(3)	2.049(2)	Co(1)-O(3)^1	2.049(2)
Co(2)-N(8)^2	2.143(3)	Co(2)-N(8)^4	2.143(3)
Co(2)-O(1)	2.102(2)	Co(2)-O(1)^5	2.102(2)
Co(2)-O(6)^5	2.130(2)	Co(2)-O(6)	2.130(2)
N(2)-Co(1)-N(2)^1	180.00(12)	N(2)^1-Co(1)-N(5)^2	88.34(12)
N(2)-Co(1)-N(5)^3	88.34(12)	N(2)-Co(1)-N(5)^2	91.66(12)
N(2)^1-Co(1)-N(5)^3	91.66(12)	N(5)^3-Co(1)-N(5)^2	180.0
O(3)-Co(1)-N(2)^1	85.98(10)	O(3)^1-Co(1)-N(2)	85.98(10)
O(3)^1-Co(1)-N(2)^1	94.02(10)	O(3)-Co(1)-N(2)	94.02(10)
O(3)-Co(1)-N(5)^3	95.30(11)	O(3)^1-Co(1)-N(5)^2	95.30(11)
O(3)^1-Co(1)-N(5)^3	84.70(11)	O(3)-Co(1)-N(5)^2	84.70(11)
O(3)^1-Co(1)-O(3)	180.0	N(8)^2-Co(2)-N(8)^4	180.0
O(1)^5-Co(2)-N(8)^2	91.95(10)	O(1)-Co(2)-O(8)^2	88.05(10)
O(1)^5-Co(2)-N(8)^4	88.05(10)	O(1)-Co(2)-N(8)^4	91.95(10)

O(1)-Co(2)-O(1)^5	180.0	O(1)^5-Co(2)-O(6)	90.95(9)
O(1)-Co(2)-O(6)	89.05(9)	O(1)^5-Co(2)- O(6)^5	89.05(9)
O(1)-Co(2)-O(6)^5	90.95(9)	O(6)-Co(2)-N(8)^4	89.32(11)
O(6)^5-Co(2)-N(8)^4	90.68(11)	O(6)^5-Co(2)-N(8)^2	89.32(11)
O(6)-Co(2)-N(8)^2	90.68(11)	O(6)-Co(2)-O(6)^5	180.0

Symmetry codes: [1]: -x, 1-y, 1-z. [2]: 1-x, 1-y, 1-z. [3]: -1+x, +y, +z. [4]: -1+x, -1+y, 1+z. [5]: -x, -y, 2-z.

Table S3. Comparison of literature reports for CPs/MOFs as sensors for Pb^{2+} and Al^{3+} detection.

Luminescent material	Analyte	Detection mechanism	K_{sv}/M^{-1}	Detection limit	Reference
ZIF-8	Pb^{2+}	Turn-off	5.87×10^4	13.07 nM	S1
CDs/QDs@ZIF-8	Pb^{2+}	Turn-off	8.46×10^4	2.35 nM	S1
ZnTCPP-MOF	Pb^{2+}	Turn-off	1.6×10^5	2.16×10^{-5} M	S2
$[Ln_2(FDC)_3L(H_2O)_3]\cdot 4.5H_2O$	Pb^{2+}	Turn-on	2.97×10^3	8.22×10^{-6} M	S3
Zn (II)-MOF	Pb^{2+}	Turn-off	1.18×10^4	8.00×10^{-7} M	S4
$[Zn(HL)(bipy)_{0.5}(H_2O)]\cdot 2H_2O$	Pb^{2+}	Turn-off	1.18×10^4	0.8 μM	S4
Tb-L	Pb^{2+}	Turn-on	----	3.43×10^{-7} M	S5
MIL-101-NH_2	Pb^{2+}	Turn-off	2.2714	5.20×10^{-7} M	S6
Tb-MOF	Pb^{2+}	Turn-off	1.75×10^4	3.40×10^{-7} M	S7
$[Tb(L)(H_2O)_5]_n$ ·solvents	Pb^{2+}	Turn-off	1.75×10^4	3.4×10^{-7} M	S7
$\{[Tb(dppa)(H_2O)_2]\cdot dima\cdot H_2O\cdot 0.5O\}_n$	Pb^{2+}	Turn-on	8.691×10^3	0.45 μM	S8

LMOF-263	Pb^{2+}	Turn-off	5.5017×10^4	19.7 ppb	S9
$[Tb(ppda)(npdc)_{0.5}(H_2O)_2]_n$	Pb^{2+}	Turn-on	1.05×10^5	9.44×10^{-5} M	S10
$[Eu(TTA)_3(2\text{-pyr})(H_2O)]$	Pb^{2+}	Turn-off	2.3×10^3	6.03 μM	S11
MOF-5	Pb^{2+}	Turn-on	18.58	0.002 μM	S12
Ru(II)@HPU-23	Pb^{2+}	Turn-on	----	52.4 nM	S13
$\{[Zn_2(1,4\text{-ndc})_2(3\text{-abpt})]\cdot2DMF\}_n$	Al^{3+}	Turn-on	6.98×10^4	----	S14
$\{[Cd(1,4\text{-ndc})(3\text{-abit})]\cdot H_2O\}_n$	Al^{3+}	Turn-on	3.84×10^4	----	S14
$[Zn_2(oba)_2(bpta)]\cdot(DMF)_3\}_n$	Al^{3+}	Turn-on	1.40×10^3	0.0012 mM	S15
Zn(DMA)(TBA)	Al^{3+}	Turn-on	1.33×10^4	1.97 μM	S16
$[Co(OBA)(DATZ)_{0.5}(H_2O)]$	Al^{3+}	Turn-on	----	2.5 μM	S17
$\{[Zn_2(OH)(Br\text{-}1,4\text{-}bdc)_{1.5}(Cz\text{-}3,6\text{-}bpy)]\cdot0.5H_2O\}_n$	Al^{3+}	Ratiometric Turn-off	5.71×10^3	0.59 μM	S18
$\{[Zn_2(OH)(Br\text{-}1,4\text{-}bdc)_{1.5}(Cz\text{-}Pr\text{-}3,6\text{-}bpy)]\cdot0.5H_2O\}_n$	Al^{3+}	Ratiometric Turn-off	5.88×10^3	1.89 μM	S18
$[Zn(H_2dhbdc)(Cz\text{-}3,6\text{-}bpy)]_n$	Al^{3+}	Turn-on	4.3×10^3	0.62 μM	S19
LCU-112	Pb^{2+}	Ratiometric Turn-on	3.57×10^5	0.1688 μM	this work
LCU-112	Al^{3+}	Ratiometric Turn-on	4.11×10^4	1.7385 μM	this work

Table S4. Comparison of literature reports for CPs/MOFs as sensors for Tb^{3+} detection.

Luminescent material	Analyte	Detection mechanism	K_{sv}/M^{-1}	Detection limit	Reference
BTC-1	Tb^{3+}	Turn-on	----	8 ± 1 ppb	S20
BTC-2	Tb^{3+}	Turn-on	----	13 ± 2 ppb	S20
BTC-3	Tb^{3+}	Turn-on	----	10 ± 1 ppb	S20
BPDC-1	Tb^{3+}	Turn-on	----	8.3 ± 0.8 ppb	S20
BPDC-2	Tb^{3+}	Turn-on	----	5.7 ± 0.6 ppb	S20
BPDC-3	Tb^{3+}	Turn-on	----	10 ± 2 ppb	S20
BioMOF-100	Tb^{3+}	Turn-on	33.09	90 ± 3 ppb	S21
HNU-25	Tb^{3+}	Turn-on	----	3×10^{-11} M	S22
HNU-26	Tb^{3+}	Turn-on	----	2×10^{-9} M	S22
CP1	Tb^{3+}	Turn-on	----	1.20 nM	S23
LCU-112	Tb^{3+}	Turn-on	4.80×10^5	0.046 μM	this work

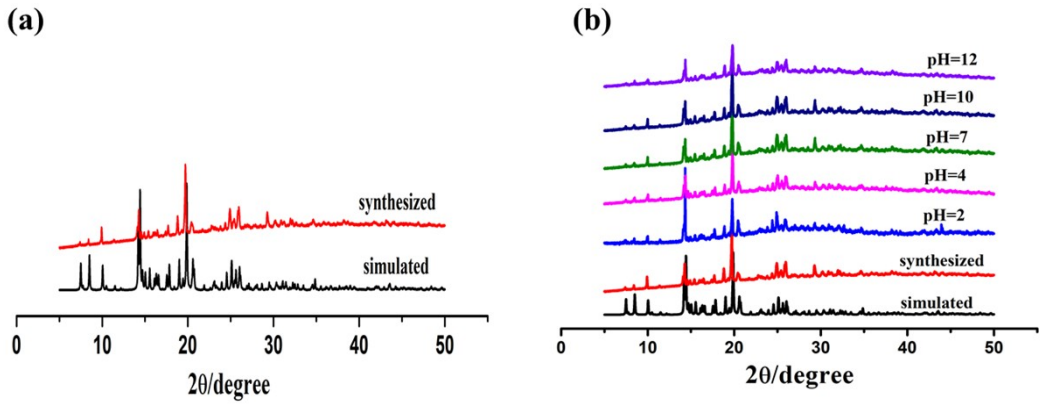

Fig. S1 (a) PXRD of **LCU-112**. (b) PXRD of **LCU-112** soaked in aqueous solution of different pH for three days.

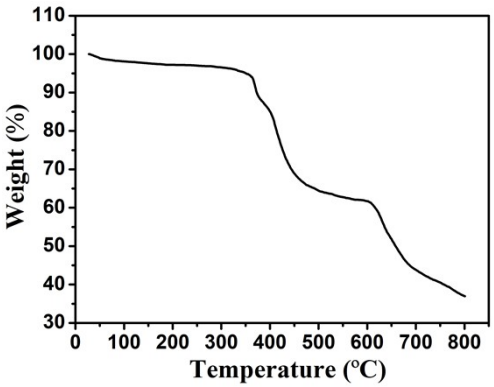

Fig. S2 TG of **LCU-112**.

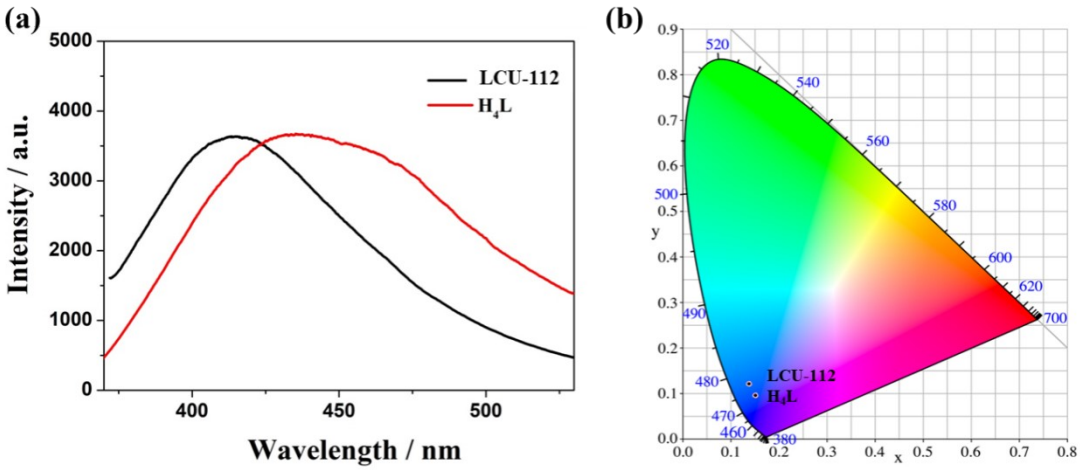

Fig. S3 (a) The solid-state luminescence spectra of **LCU-112**. (b) The CIE coordinates of **LCU-112** and H_4L.

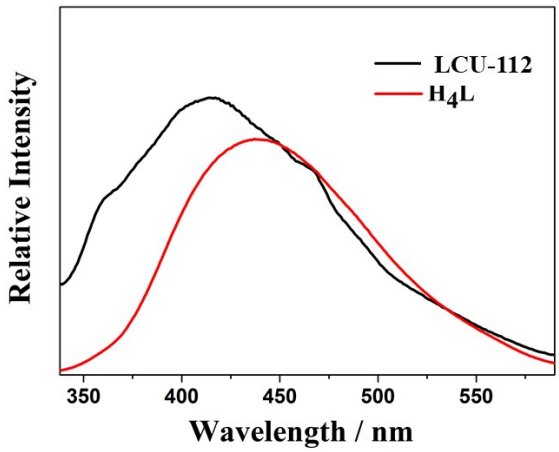

Fig. S4 The emission spectra of **LCU-112** and H_4L in aqueous solution.

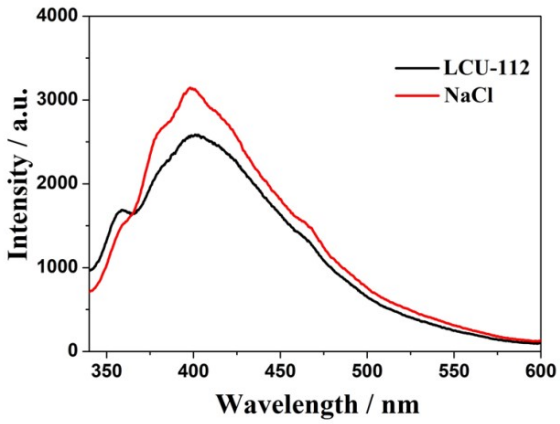

Fig. S5 Luminescence spectra of **LCU-112** dispersed in NaCl.

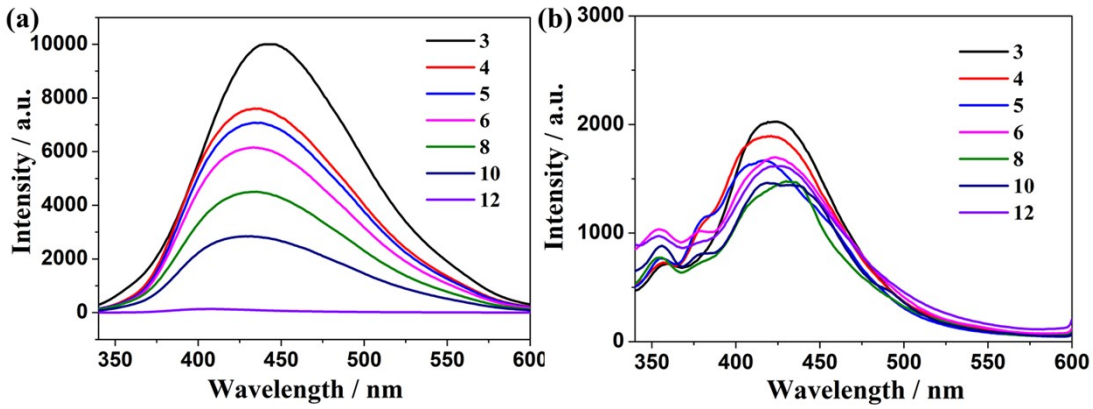

Fig. S6 Luminescence spectra of $\mathbf{H_4L}$ and tttmb at different pH values.

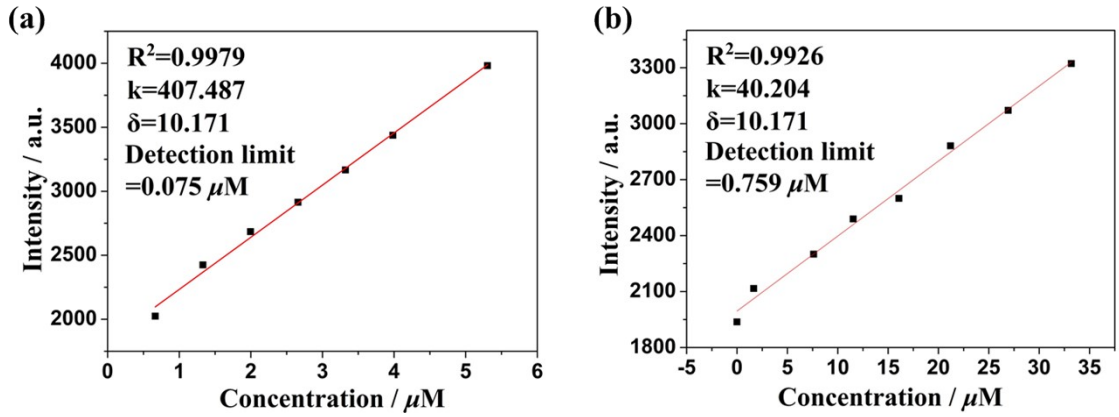

Fig. S7 (a) and (b) The detection limit of **LCU-112** toward Pb^{2+} and Al^{3+} in aqueous suspensions of **LCU-112**.

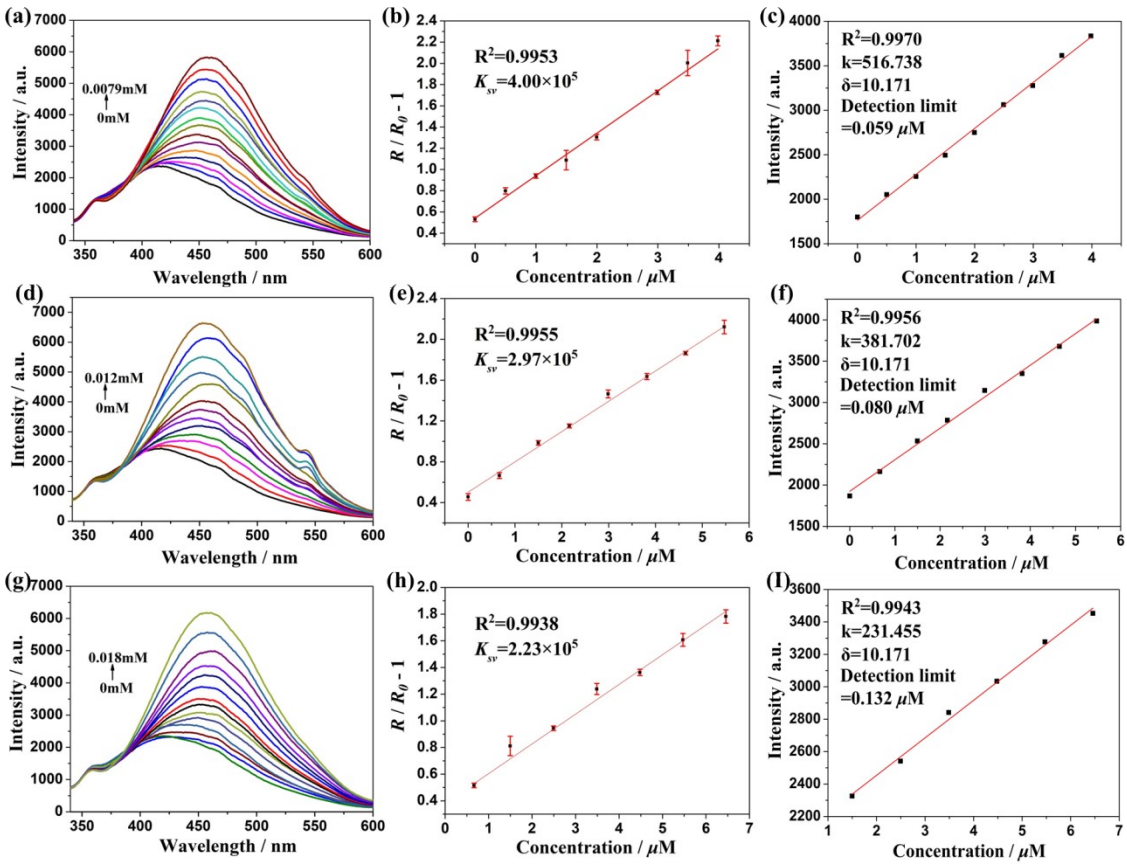

Fig. S8 (a) (d) (g) Luminescence titration result of **LCU-112** toward Pb^{2+} at pH = 5, 6, 7. (b) (e) (h) The K_{sv} of **LCU-112** toward Pb^{2+} at pH = 5, 6, 7. (c) (f) (I) The detection limit of **LCU-112** toward Pb^{2+} at pH = 5, 6, 7.

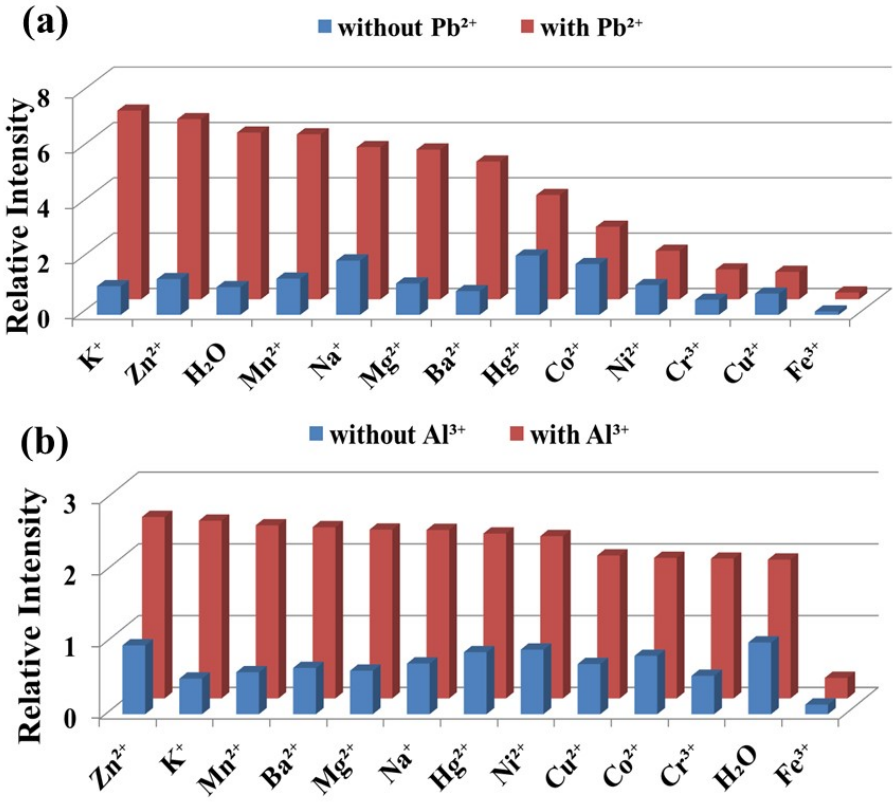

Fig. S9 (a) and (b) Comparison of luminescence intensity of the chemicals with and without presence of Pb^{2+} and Al^{3+} at 415 and 460 nm, respectively.

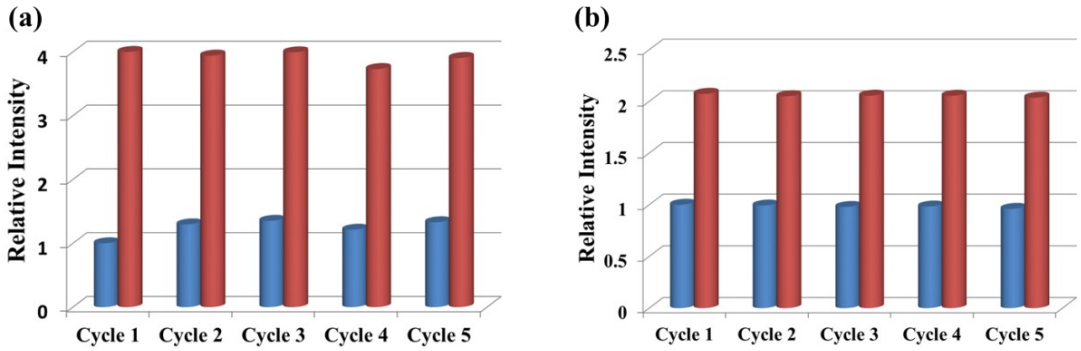

Fig. S10 (a) and (b) The recycling experimental of Pb^{2+}, Al^{3+} within five runs.

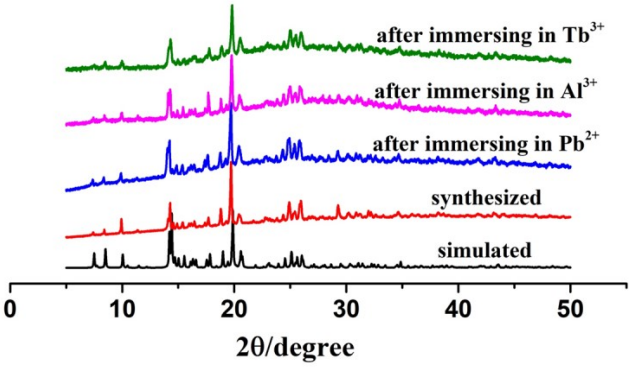

Fig. S11 PXRD of **LCU-112** soaked in aqueous solutions containing Pb^{2+}, Al^{3+} and Tb^{3+} for three days.

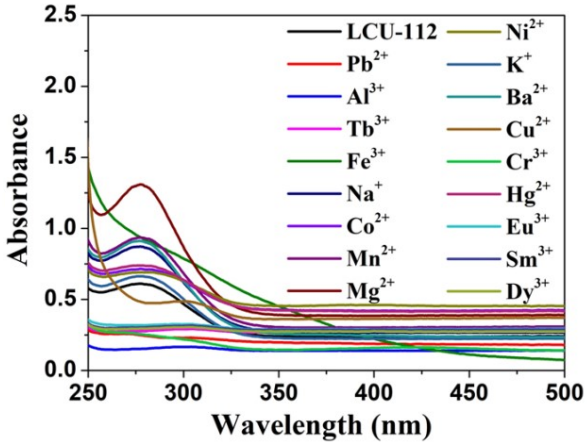

Fig. S12 UV−vis absorption spectra of **LCU-112** upon the addition of various cations.

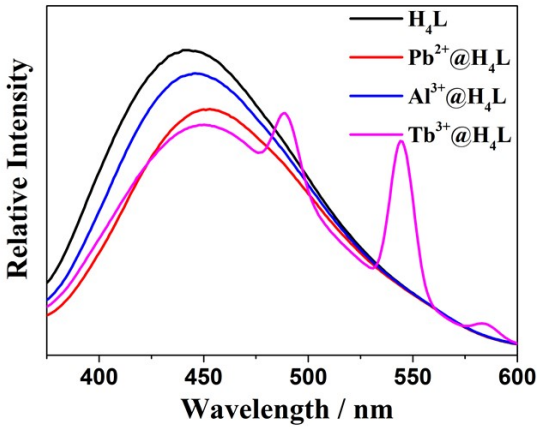

Fig. S13 Luminescence spectra of H_4L ligand in aqueous solutions with Pb^{2+}, Al^{3+} and Tb^{3+}.

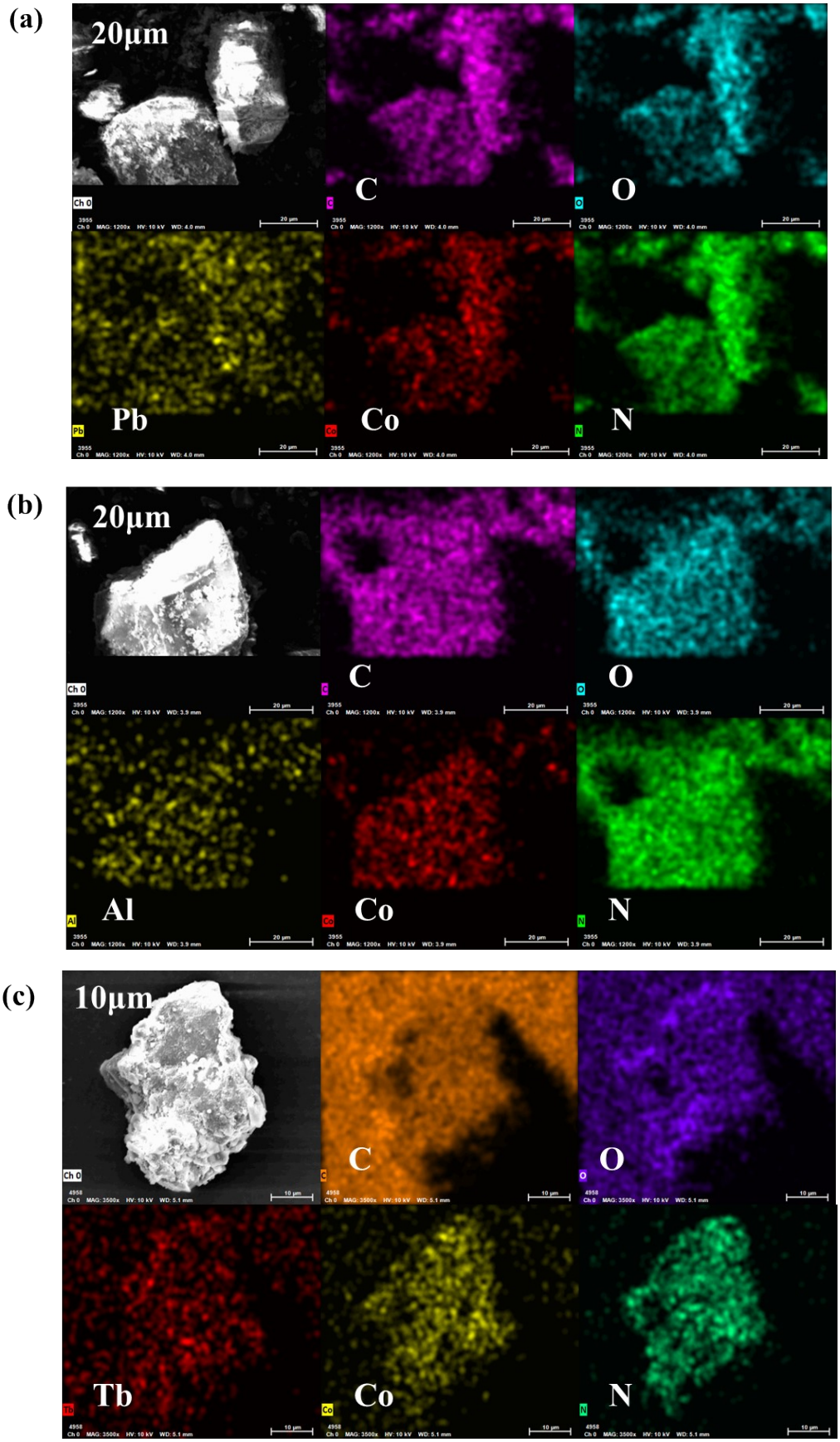

Fig. S14 (a)-(c) The EDS mapping results of **LCU-112** after immersing in Pb^{2+}, Al^{3+} and Tb^{3+}, showing the uniform distribution of all elements.

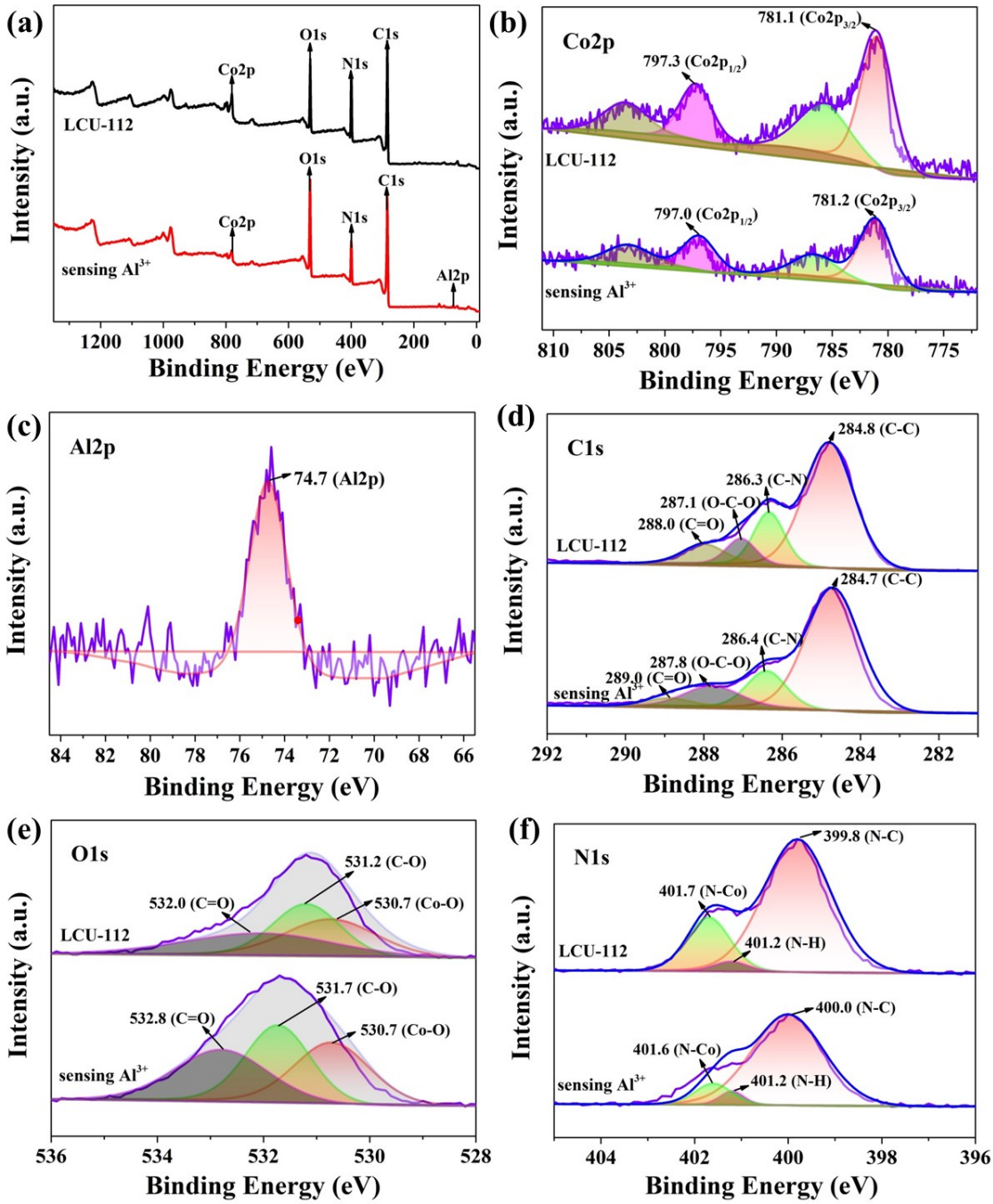

Fig. S15 (a) XPS spectra of **LCU-112** before and after immersion in Al^{3+}. (b)-(f) High resolution regions of Co2p, Al2p, C1s, O1s and N1s.

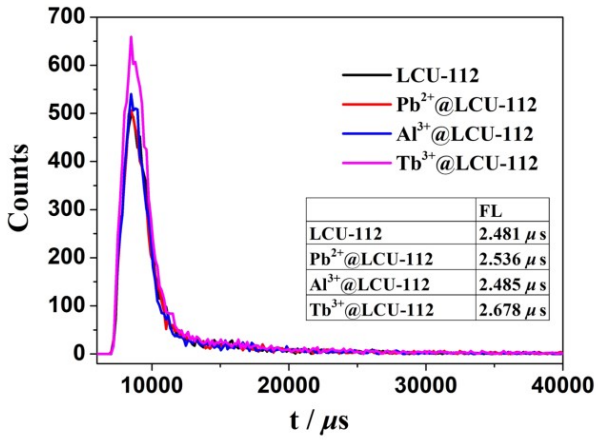

Fig. S16 The luminescence decay lifetimes of the original **LCU-112** and after soaked in aqueous solutions of Pb^{2+}, Al^{3+} and Tb^{3+}.

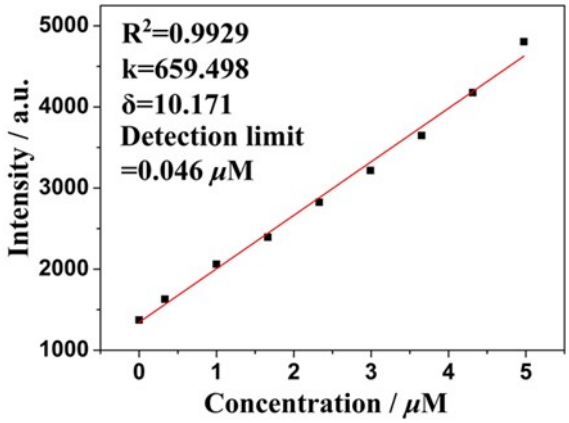

Fig. S17 The detection limit of **LCU-112** toward Tb^{3+}.

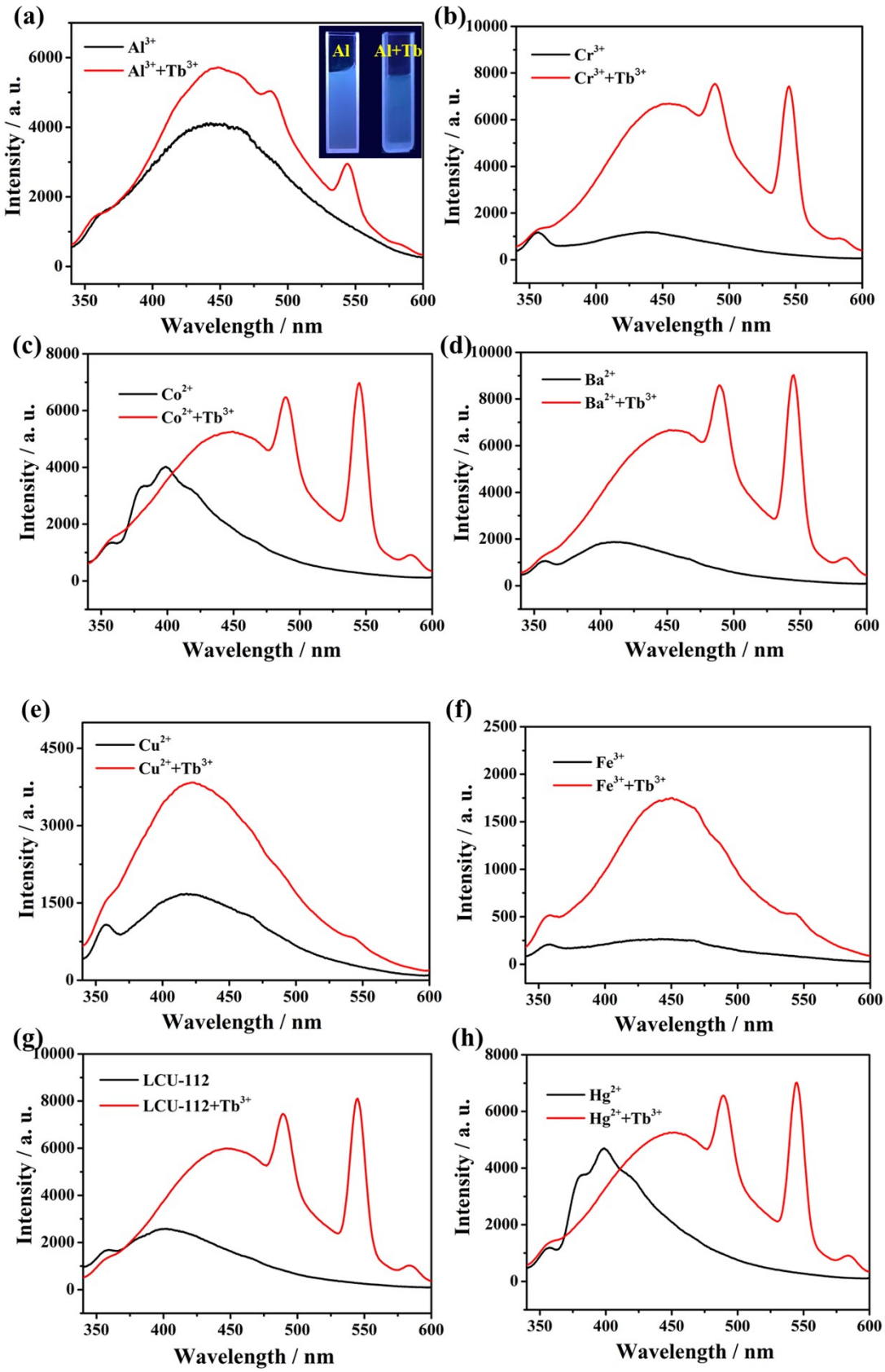
(a)
Al3+
Al3++Tb3+
Al
Al+Tb
Intensity / a. u.
Wavelength / nm
(b)
Cr3+
Cr3++Tb3+
(c)
Co2+
Co2++Tb3+
(d)
Ba2+
Ba2++Tb3+
(e)
Cu2+
Cu2++Tb3+
(f)
Fe3+
Fe3++Tb3+
(g)
LCU-112
LCU-112+Tb3+
(h)
Hg2+
Hg2++Tb3+

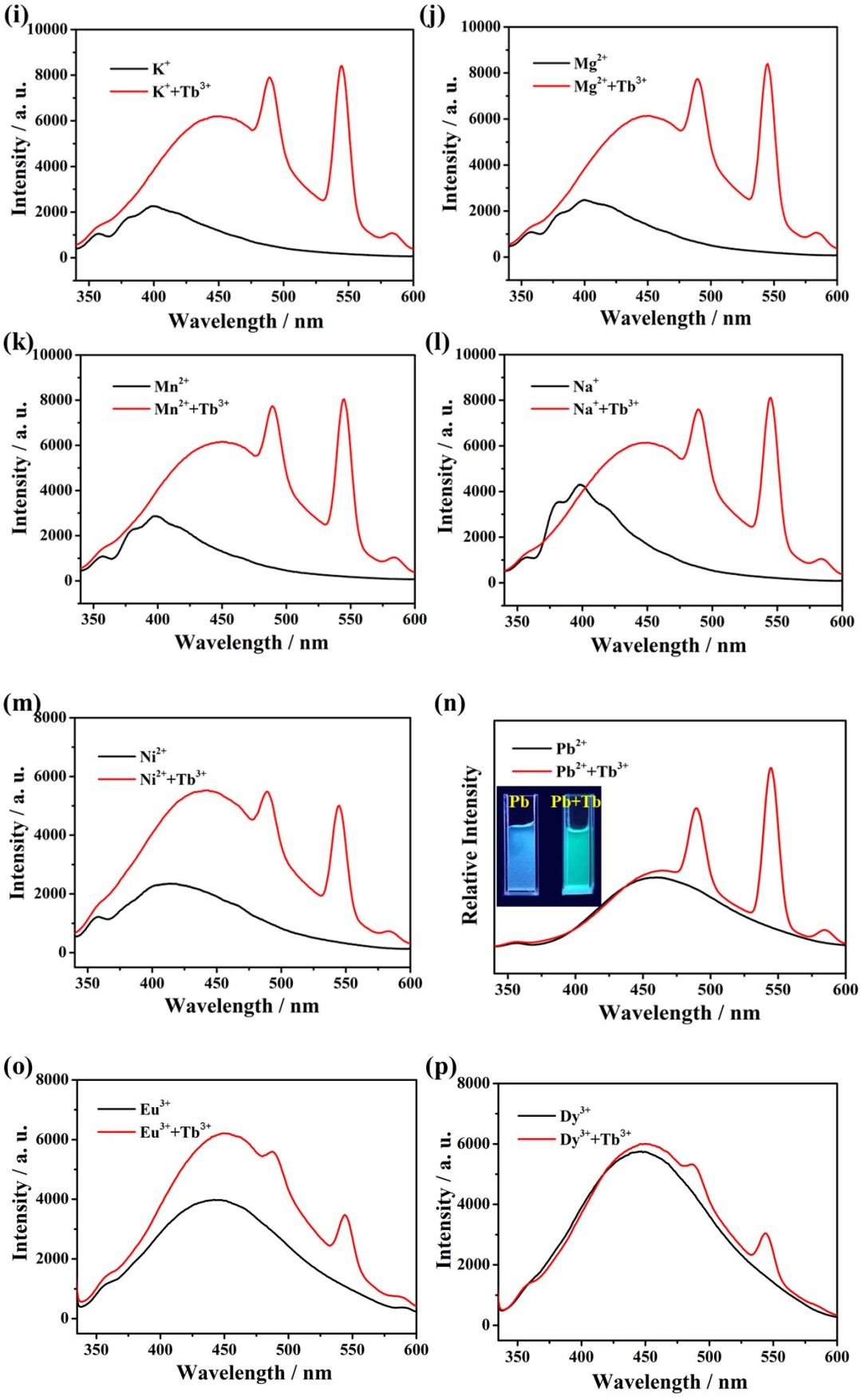
(i)
Intensity / a. u.
Wavelength / nm
K+
K+ +Tb3+
(j)
Mg2+
Mg2+ +Tb3+
(k)
Mn2+
Mn2+ +Tb3+
(l)
Na+
Na+ +Tb3+
(m)
Ni2+
Ni2+ +Tb3+
(n)
Relative Intensity
Pb2+
Pb2+ +Tb3+
Pb
Pb+Tb
(o)
Eu3+
Eu3+ +Tb3+
(p)
Dy3+
Dy3+ +Tb3+

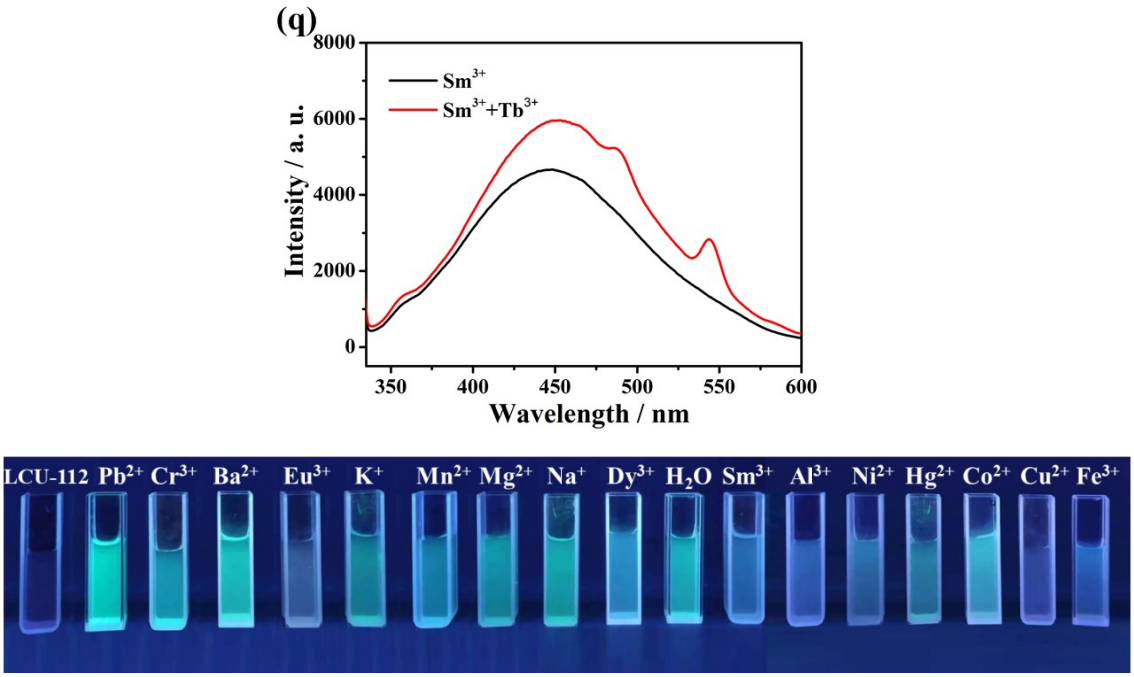

Fig. S18 The luminescence emission of **LCU-112** in aqueous solutions containing different cations with the absence and presence of Tb^{3+} and Photo by 254 nm UV lamp.

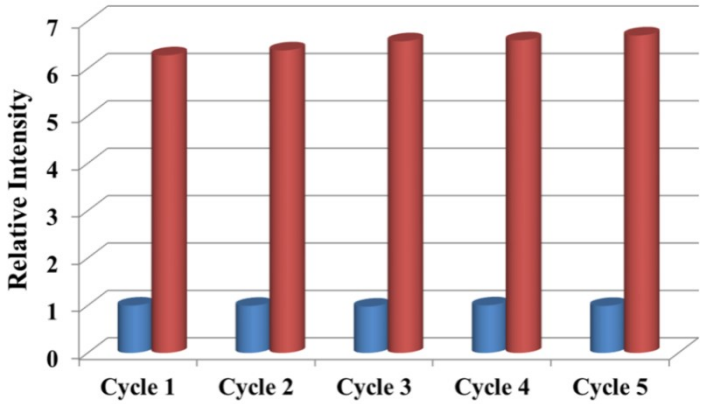

Fig. S19 The recycling experimental of Tb^{3+} within five runs.

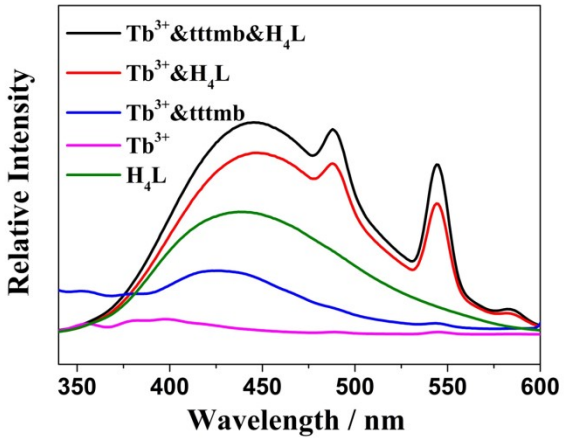

Fig. S20 Luminescence spectra of H_4L ligand and tttmb in aqueous solutions with Tb^{3+}.

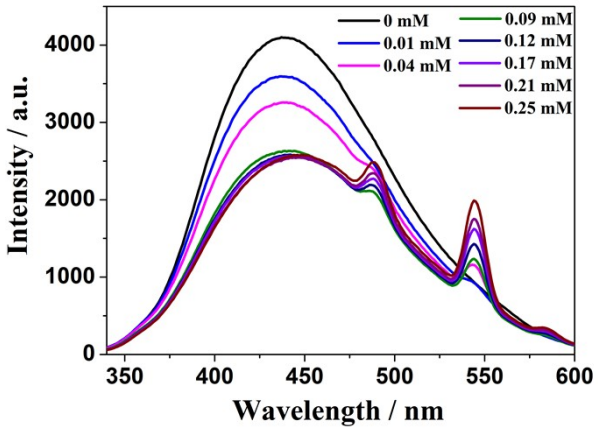

Fig. S21 The titration experiment of Tb^{3+} solution into H_4L.

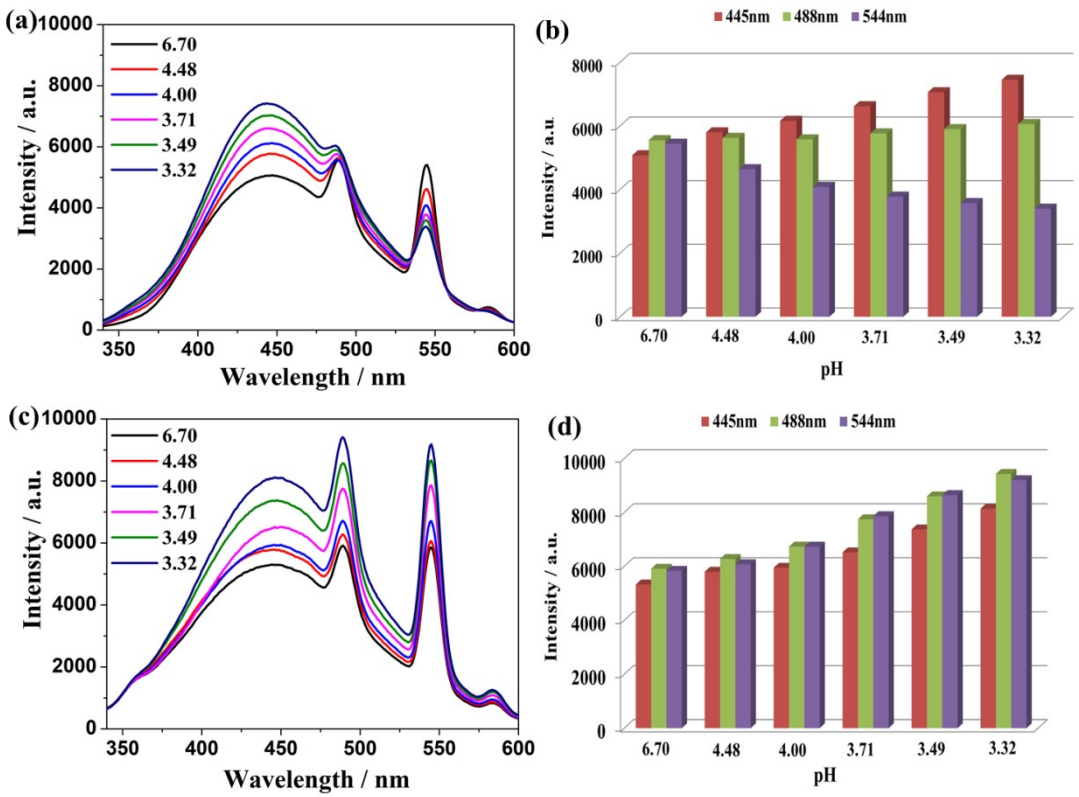

Fig. S22 (a) and (b) Fluorescence diagram and histogram of Tb^{3+} fluorescence sensing by H_4L under different pH conditions. (c) and (d) Fluorescence diagram and histogram of Tb^{3+} fluorescence sensing by **LCU-112** under different pH conditions.

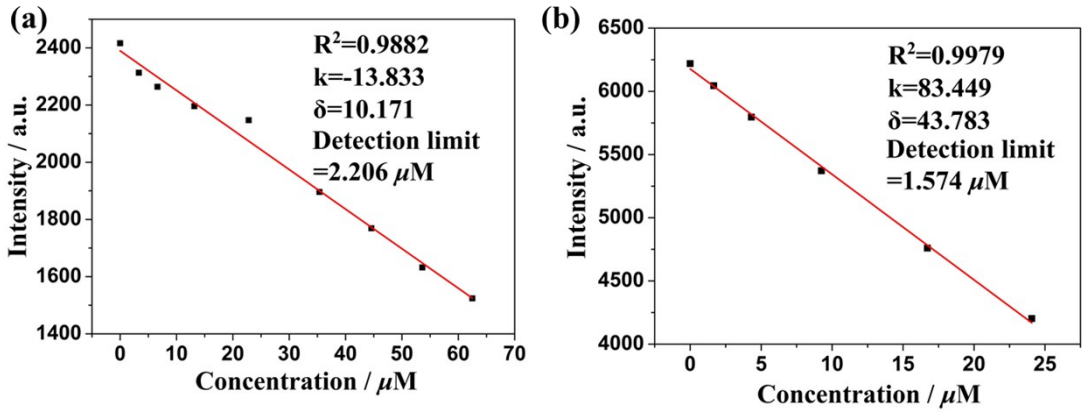

Fig. S23 (a) and (b) The detection limit of **LCU-112** and **Tb^{3+}@LCU-112** toward Fe^{3+}.

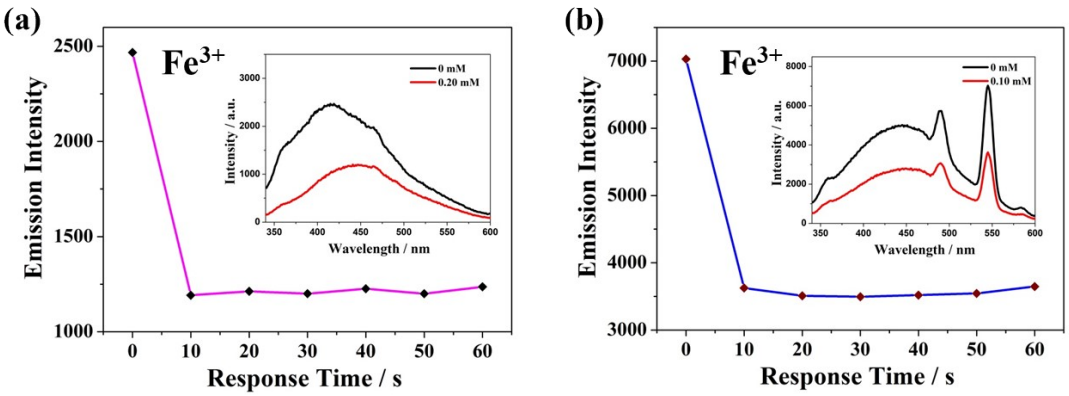

Fig. S24 The time-dependent response of **LCU-112** and **Tb^{3+}@LCU-112** after adding Fe^{3+}.

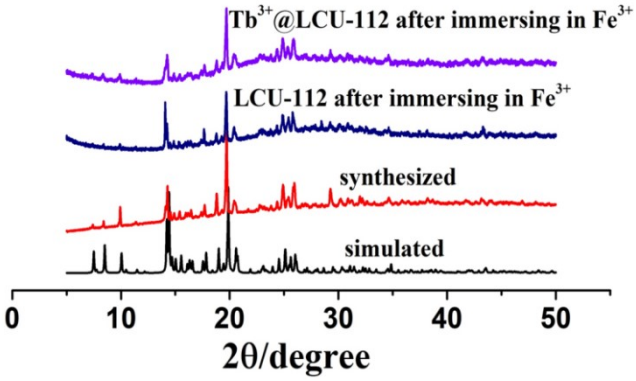

Fig. S25 PXRD of **LCU-112** and **Tb^{3+}@LCU-112** soaked in aqueous solutions containing Fe^{3+} for three days.

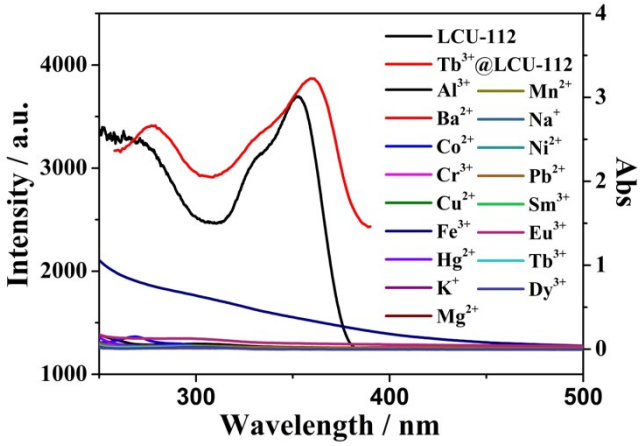

Fig. S26 The excitation of **LCU-112** and **Tb^{3+}@LCU-112** and UV–Vis spectra of cations.

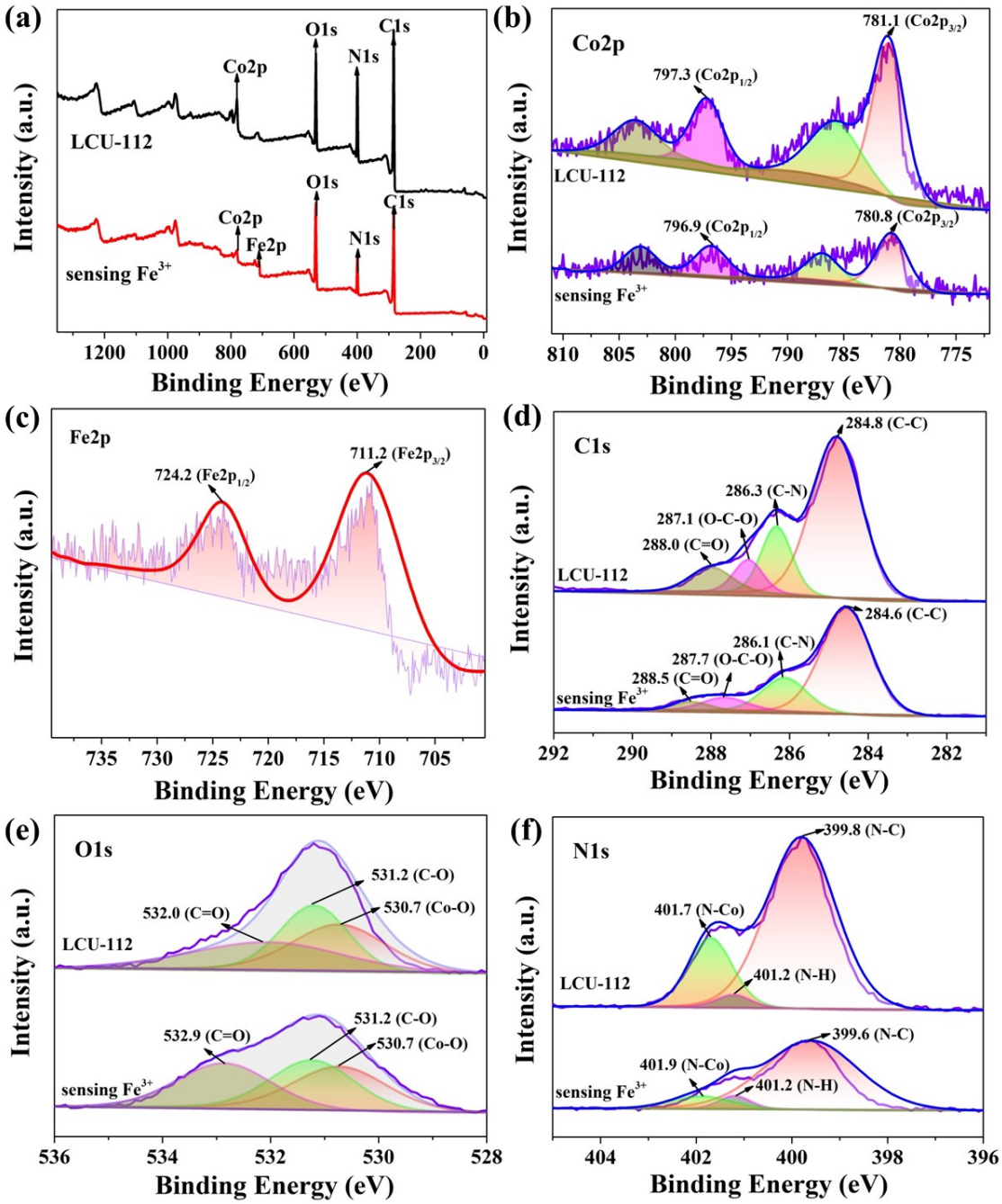

Fig. S27 (a) XPS spectra of **LCU-112** before and after immersion in Fe^{3+}. (b)-(f) High resolution regions of Co2p, Fe2p, C1s, O1s and N1s.

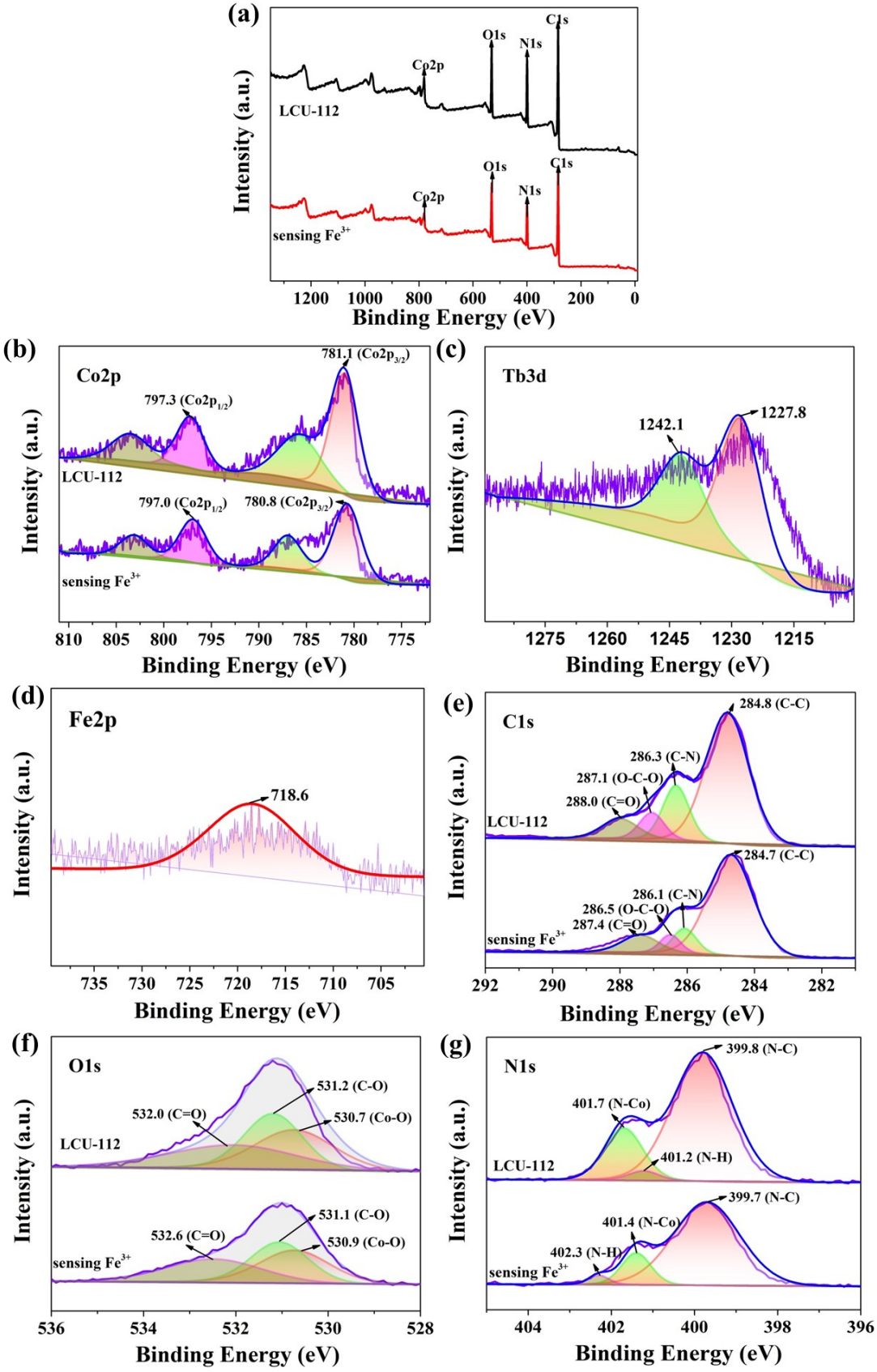

Fig. S28 (a) XPS spectra of **Tb^{3+}@LCU-112** before and after immersion in Fe^{3+}. (b)-(g) High resolution regions of Co2p, Tb3d, Fe2p, C1s, O1s and N1s.

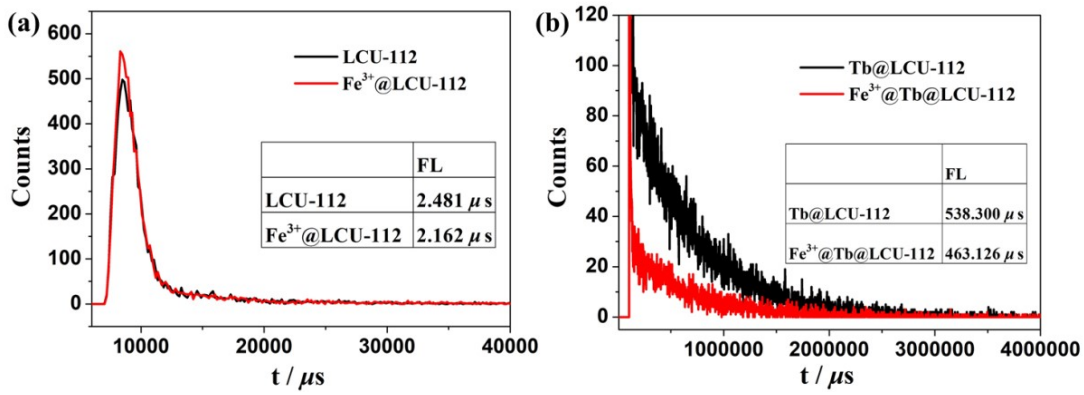

Fig. S29 (a) The luminescence decay lifetimes of the original **LCU-112** and after soaked in aqueous solutions of Fe^{3+}, (b) The luminescence decay lifetimes of **Tb^{3+}@LCU-112** and after soaked in aqueous solutions of Fe^{3+}.

References

S1 K. Y. Yi, L. Zhang, *Journal of Hazardous Materials*, 2020, **389**, 122141.

S2 Q. Y. Wang, W. Q. Ke, H. Y. Lou, *Dyes and Pigments*, 2021, **196**, 109802.

S3 L. Li, Q. Chen and Z. G. Niu, *J. Mater. Chem. C*, 2016, **4**, 1900-1905.

S4 J. X. Hou, J. P. Gao and J. Liu, *Dyes Pigm*., 2019, **160**, 159-164.

S5 B. Xu, X. Tang and J. Zhou, *Dalton Trans*., 2016, **45**, 18859-18866.

S6 S. W. Lv, J. M. Liu and C. Y. Li, *Chem. Eng. J*., 2019, **375**, 122111.

S7 G. F. Ji, J. J. Liu and X. C. Gao, *J. Mater. Chem. A*, 2017, **5**, 10200-10205.

S8 X. L, Chen, L. Shang and L. Liu, *Dyes and Pigm*., 2021, **196**, 109809.

S9 N. D. Rudd, H. Wang and E. M. A. *ACS Appl. Mater. Interfaces*, 2016, **8**, 30294-30303.

S10 Z. Li, Z. Y. Zhan and M. Hu, *CrystEngComm*, 2020, **22**, 6727-6737.

S11 C. J. Macrino, A. S. Borges and A. C. Neto, *J. Braz. Chem. Soc*., 2022, **2**, 173-182.

S12 S. F. Xu, L. H. Zhan and C. Y. Hong, *Sens. Actuators B Chem*., 2020, **308**, 127733.

S13 X. Xu, H. J. Li and Z. Q. Xu, *Chem. Eng. J*., 2022, **436**, 135028.

S14 J. Zhang, L. Gong and J. Feng, *New J. Chem*., 2017, **41**, 8107-8117.

S15 E. Khezerloo, S. M. Mousavi-khoshdel and V. Safarifard, *Polyhedron,* 2019, **166**, 166-174.

S16 X. Zhang, X. Luo, N. Zhang, J. Wu and Y. Q. Huang, *Inorg. Chem. Front*., 2017, **4**, 1888-1894.

S17 D. T. Singha, P. Mahata, *Inorg. Chem*., 2015, **54**, 6373-6379.

S18 P. M. Chuang, Y. W. Huang and Y. L. Liu, *CrystEngComm*, 2021, **23**, 2222-2234.

S19 W. T. Chen, M. J. Tsai and J. Y. Wu, *Cryst. Growth Des*., 2022, **22**, 228-236.

S20 X. Gao, G. Sun, F. Ge and H. Zheng, *Inorg. Chem*., 2019, **58**, 8396-8407.

S21 X. X. Liu, L. P. Lu and M. L. Zhu, *Sens. Actuators B Chem*., 2021, **347**, 130641.

S22 J. Y. An, C. M. Shade, D. A. Chengelis-Czegan, S. Petoud and N. L. Rosi, *J. Am. Chem. Soc*., 2011, **133**, 1220-1223.

S23 M. L. Li, G. J. Ren, F. X. Wang, Z. M. Li, W. T. Yang, D. X. Gu, Y. H. Wang, G. S. Zhu and Q. H. Pan, *Inorg. Chem. Front.*, 2019, **6**, 1129-1134.